# F-16 FOREBODY VORTEX CONTROL

Brooke C. Smith
*Eidetics International, Inc.,*
*Torrance, California 90505*

## SUMMARY

Low-speed F-16 wind tunnel tests have been completed for the purpose of evaluating pneumatic and mechanical yaw control devices at high angles of attack. The performance of tangential jet and slot blowing was evaluated with three different forebody configurations — the standard nose, the standard nose with a chine, and an elliptical cross-section nose (the shark nose). Variations to the jet geometry included: azimuth angle and longitudinal placement. It was found that jets angled across the forebody were most effective and there is an optimum region for influencing the flowfield. Different slot lengths, longitudinal positions and radial locations were also investigated. Jets were more efficient yaw moment effectors than slots at the same mass flow. The mechanical rotating nose boom strake performance was evaluated with only the standard and shark noses. Variations to the strakes included: single and dual strakes, planform shape, longitudinal placement, and included angle for the dual strake configuration. The strake performance was relatively unaffected by the strake geometry, though longitudinal placement on the nose boom changed the fluid dynamic interactions.

## INTRODUCTION

The standard F-16 configuration develops a directional instability at angles of attack above 30° as shown in Fig. 1. Compounding the problems associated with the loss of static stability is a simultaneous decrease in directional control power that precludes the use of an active stability augmentation system. As a result, the current F-16 flight control system limits the angle of attack thereby avoiding the problem area and does not fully realize the maximum lift and maneuver performance potential of the aircraft.

Two techniques to remove the limitation present themselves. If sufficient yaw control power was available, it would be possible to overcome the loss of directional stability without modification of the standard nose. Or a modified forebody geometry could passively restore the aircraft's stability without relying on an active control system. These approaches are not necessarily mutually exclusive. An active control system would benefit from a less unstable platform and a passive fix would still require additional control power for maneuvering at high angles of attack.

This paper summarizes results of an investigation of yaw control at high angles of attack with the standard F-16 forebody, a modified forebody incorporating a chine, and an elliptical cross-section nose (the "shark" nose). The pneumatic control systems consist of a pair of small jets or slots oriented to blow tangentially across the surface of the nose. The experimental series for each nose geometry covered a variety of longitudinal positions on the nose and different nozzle azimuth angles. The mechanical control system consists of one or two small strakes that rotate about the nose boom, shedding small vortices, which interact with the forebody flowfield. The experimental series for each nose geometry covered a variety of strake planforms, different longitudinal locations on the nose boom, and dihedral angles.

## MODEL AND EXPERIMENTAL SET-UP

### Configuration Description

A structurally reinforced 10% spin tunnel F-16 model was used and is shown in Fig. 2. The model included the engine inlet as a straight flow-through duct. The leading-edge flap deflection was 25°. In all figures presented in this report, the moment reference center is 35% mac, and the reference dimensions used for data reduction correspond to the full configuration. The data are shown in body axes.

The chine nose configuration was modeled by adding a flat-plate chine to the standard nose. The chine planform, designated as the 7m configuration, was developed by the U. S. Air Force to improve the directional stability characteristics of the F-16 and is sketched in Fig. 3. The elliptical cross-section nose, designed by Eidetics, resembles the F-5 shark nose. Lines of the standard F-16 and shark noses are shown in Figs. 4 and 5, respectively.

---

* Senior Engineer, Senior Member AIAA.

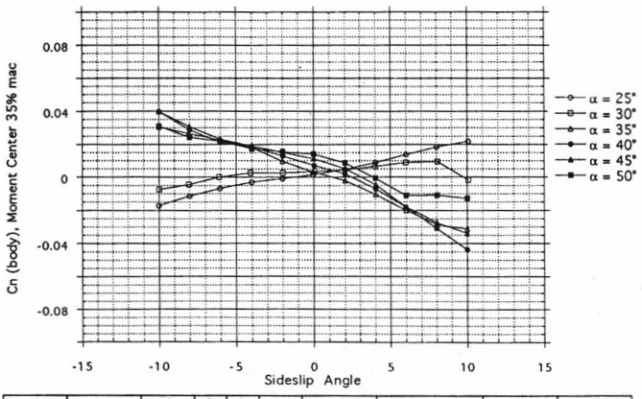


| RUN# | α | β | δφ | δμ | qbar | Forebody | FVC Designation | Other | Comments |
|---|---|---|---|---|---|---|---|---|---|
| 788-793 | 25° to 50° | sweep | --- | --- | 20 | STANDARD | none | std LEX, SB | |

**Figure 1. Standard F-16 Yaw Instability**

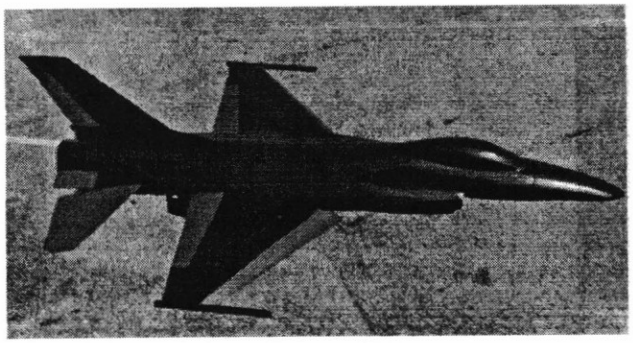

**Figure 2. 10% F-16 Wind Tunnel Model**

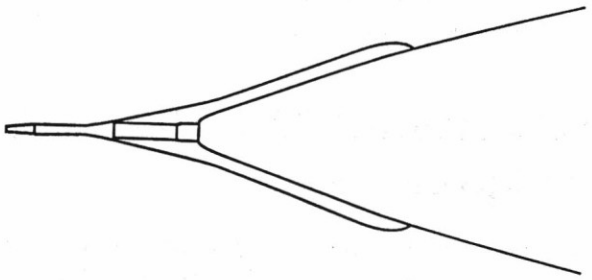

**Figure 3. USAF 7m Chine Planform**

The profile of the shark nose is identical to the standard nose; the cross sections are blended so they match the standard F-16 contours at FS 62.5.

## Facility and Instrumentation

Primary testing was done at NASA Langley in the 14x22 foot wind tunnel. Angles of attack for the tests ranged from 0° to 60° with a straight sting. Blockage and wall corrections were made in spite of the relatively small size of the model. The majority of the tests were performed at a dynamic pressure of 20 psf. The model was equipped with a 6-component force and moment balance, surface pressure measurements, pneumatic supply pressure transducers and thermocouples. Exploratory wind tunnel tests at the University of Toledo 3x3 foot wind tunnel used a partial model of the F-16 forward fuselage[1,2].

## CLEAN FOREBODY, α EFFECTS w/o FVC

The yaw moment behavior of the standard F-16 configuration at fixed angles of attack was shown previously in Fig. 1. The same configuration is shown in angle of attack sweeps at fixed sideslips in Fig. 6. The increment between the 0° and ±4° sideslip curves shows static directional stability. The crossing of the curves above 30° AOA is readily apparent. The 0° curve shows a large asymmetry developing at above 40° AOA that is not apparent with the other nose shapes. This yaw moment is due to asymmetric separation and vortex formation on the nose. By providing a more definite location for cross-flow separation, the chine and shark noses minimize the asymmetric flow. The addition of the chine removes the yaw instability and eliminates the large asymmetry at high AOA as shown in Fig. 7. The shark nose effect on the

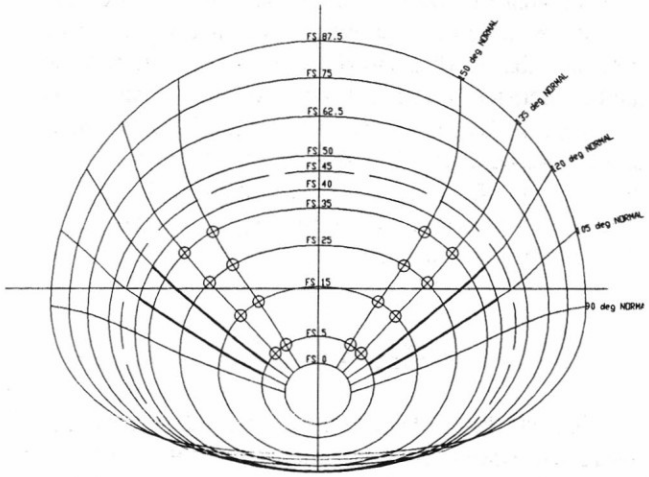


**Figure 4. F-16 Standard Nose Contours**

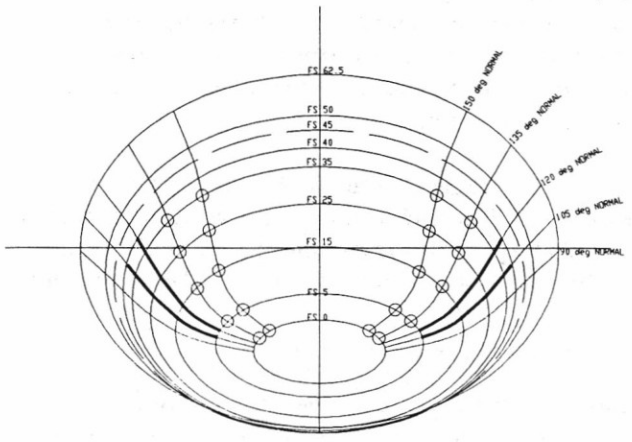


**Figure 5. Eidetics' Shark Nose Definition**

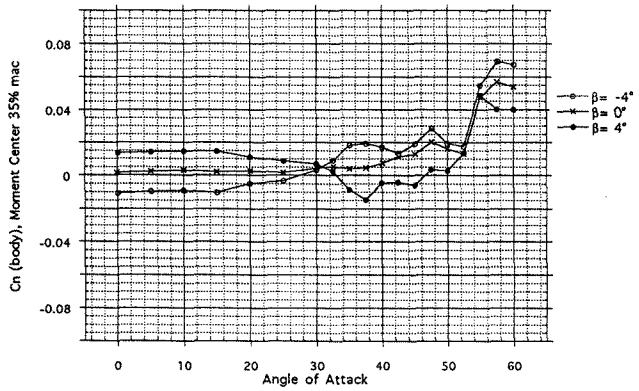


| RUN# | α | β | δφ | δμ | qbar | Forebody | FVC Designation | Other | Comments |
|---|---|---|---|---|---|---|---|---|---|
| 782-784 | sweep | -4° to 4° | --- | --- | 20 | STANDARD | none | std LEX, SB | |

**Figure 6. Standard F-16 in Pitch**

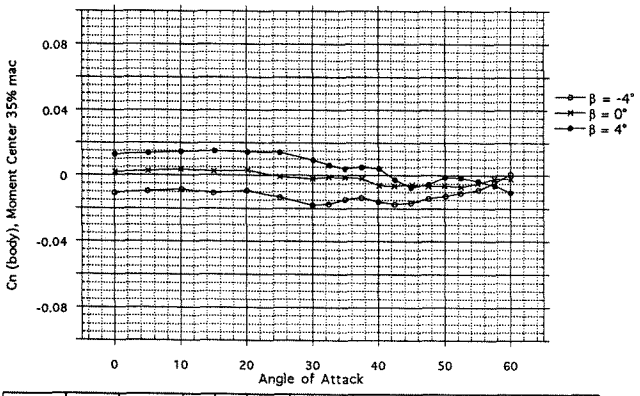


| RUN# | α | β | δφ | δμ | qbar | Forebody | FVC Designation | Other | Comments |
|---|---|---|---|---|---|---|---|---|---|
| 760-764 | sweep | -4° to 4° | --- | --- | 20 | 7m CHINE | none | LEX3, LSB | |

**Figure 7. Chine Nose F-16 in Pitch**

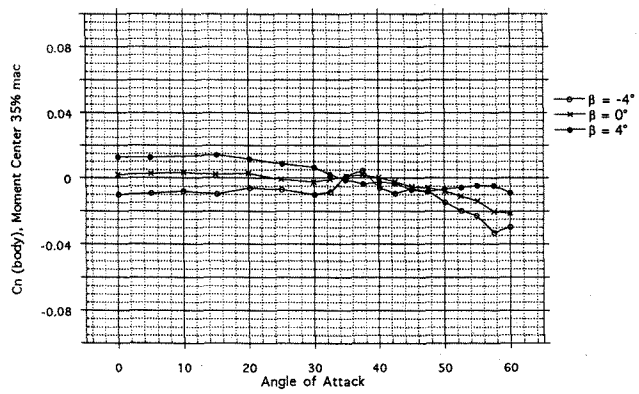


| RUN# | α | β | δφ | δμ | qbar | Forebody | FVC Designation | Other | Comments |
|---|---|---|---|---|---|---|---|---|---|
| 610-612 | sweep | -4° to 4° | --- | --- | 20 | SHARK | none | LEX3, LSB | |

**Figure 8. Shark Nose F-16 in Pitch**

yaw moment is shown in Fig. 8. These three graphs clearly show the main impetuses for considering alternate configurations for the F-16 forebody, i.e., less asymmetry and less static instability.

## PNEUMATIC FVC

Generally, the magnitude of jet or slot blowing has been expressed in terms of momentum coefficient, Cμ. This stems from the use of momentum coefficient to characterize the thrust developed by jet propulsion. In the current application, control forces are not developed directly from reactive thrust but rather by influencing the vortical flow development on the forebody.

The contribution of reaction thrust to yaw moment can be calculated by the following formula.

$$Cn|_{reactive\ thrust} = C\mu \frac{l_{jet}}{b} \sin\psi$$

$$= \frac{\dot{m} V_{jet}}{qS} \frac{l_{jet}}{b} \sin\psi$$

$$= MFR \frac{2V_{jet}}{V_\infty} \frac{l_{jet}}{b} \sin\psi$$

Values corresponding to the maximums used in these tests yields a very small ΔCn due to reactive thrust of 0.002. As will become apparent, there is a clear interaction between the jet blowing and the forebody vortices that produces yaw moments far greater than those due to the direct jet thrust effect.

Reference 3 reports on affecting wing-tip vortex formation through blowing and asserts that the momentum coefficient may not be an appropriate scaling parameter if the vortex structure is significantly altered as a result of the blowing. This observation is supported by recent forebody vortex control experiments with F/A-18[4,5]. Suspecting that Cμ may not be the best way to characterize the blowing magnitude, due to the fluid dynamic amplification, in this paper, pneumatic FVC is expressed in terms of the non-dimensional mass flow ratio (MFR), i.e., the mass flow issuing from the nozzle or slot divided by the mass flow of the freestream through the reference area. Positive MFR values denote blowing from the nozzle located on the right side of the forebody, while negative values correspond to blowing from the left side.

## STANDARD NOSE

### Jets

Investigations of forebody vortex control by small blowing jets began as early as 1979 with the F-5 and with a slender cone. More recent studies on the F-18 and X-29 have expanded on the earlier work. The X-29 work of Ref. 6 introduced the concept of rotating the jets inboard that produced much larger control moments. Reference 7 is a recent synopsis of FVC research with a number of

different aircraft. The present work attempts a parametric study of pneumatic FVC configurations on forebodies of a horizontal elliptical cross-section. The three geometries under consideration form a progression from the mild ellipse of the standard forebody to the severe "ellipse" represented by the chine configuration.

Multiple longitudinal and radial locations for the jets were built into each of the nose pieces. Nozzles could be positioned at full-scale fuselage stations (FS) of 5, 15, 25, and 35, identified by the letters B, C, D, and E, respectively. The shark nose had an additional nozzle position, A, at FS 0. Two rows of nozzle ports were built into the noses. Each row of nozzle ports followed a line where the local vectors normal to the nose surface were parallel. Only ports along the 150° normal radial line were used in these tests. The locations of the nozzle ports for the standard and shark noses are shown in Figs. 4 and 5. All nozzles could be rotated about an axis normal to the body allowing them to be pointed at any desired azimuth angle.

**Angle of Attack**. Forebody jet blowing is effective over a large angle of attack range as shown in Fig. 9. Notice that the reactive thrust component would appear less than the symbol diameter on this plot, showing the large amplification effect. As a point of comparison, at $\alpha$=0°, a 30° rudder deflection (maximum deflection) produces a $\Delta Cn = 0.045$. The rudder effectiveness is roughly constant to an angle of attack of 30° above which it falls off rapidly.

**Nozzle Azimuth**. To explore effects of the orientation of the blowing jet, the nozzle was rotated in 30° increments. The nozzle azimuth angle was defined with 0° pointing aft along the line of constant surface slope and a positive rotation as pointing inward. (Refer to Fig. 10.) For example, an azimuth of 90° means the jet was blowing across the forebody regardless of whether it was on the right or left side.

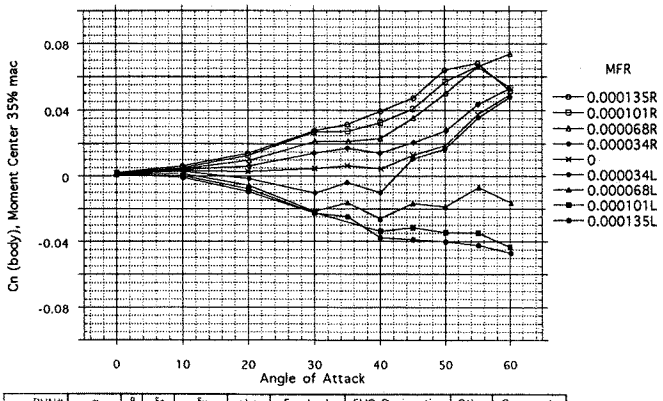


| RUN# | α | β | δφ | δμ | qbar | Forebody | FVC Designation | Other | Comments |
|---|---|---|---|---|---|---|---|---|---|
| 309-317 | sweep | 0 | --- | various | 20 | STANDARD | J150-C120 | | jets |

**Figure 9. Jet Blowing on Standard Nose**

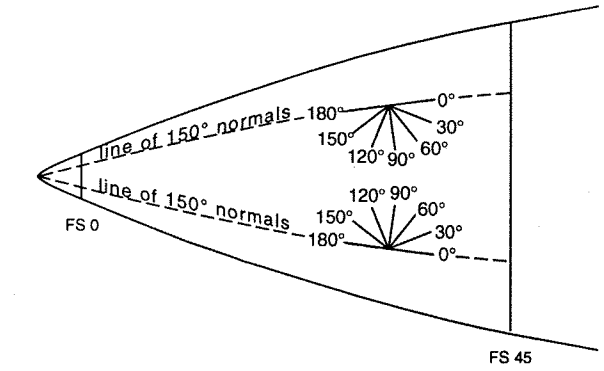


**Figure 10. Nozzle Azimuth Definition**

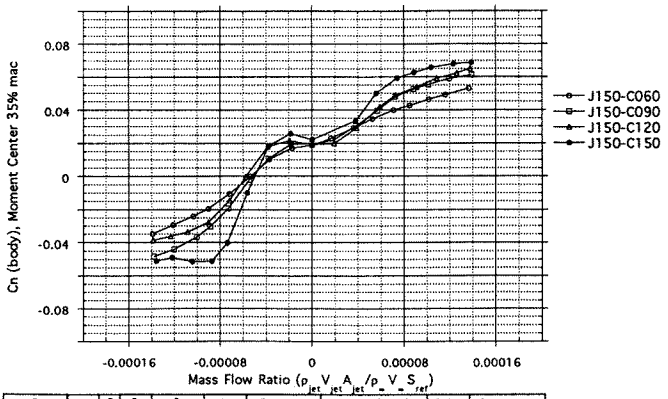


| RUN# | α | β | δφ | δμ | qbar | Forebody | FVC Designation | Other | Comments |
|---|---|---|---|---|---|---|---|---|---|
| 259-324 | 50° | 0 | --- | sweep | 20 | STANDARD | various | | jets |

**Figure 11. Effect of Nozzle Azimuth Standard Nose, FS 15**

Figure 11 shows the nozzle at FS 15 (location "C") between 60° and 150° azimuth angles. The control effectiveness increases as the nozzle turns inboard. An interesting characteristic is observed; as the nozzles rotate forward, a small reversal in effectiveness develops at low blowing rates. Using the J150-C150 configuration as an example, it can be seen that the small mass flow ratio of 0.00002 on the left side causes a yaw moment increment to the right compared to the zero blowing case. Note: The non-zero value of yaw moment developed with zero blowing is due to the naturally asymmetric flow on the forebody as discussed previously. A possible explanation for the reversal phenomenon is that the jet at low blowing rates acts more as a separator, adding momentum thickness to the boundary layer and causing earlier separation, while at higher blowing rates it acts as a flow energizer, delaying separation through a Coanda effect and entraining more flow into the opposite side vortex.

During the preliminary tests in a systematic exploration, the nozzle at FS 15 (location "C") was rotated through a complete 360° in 30° increments. All orientations with the nozzles pointing outboard showed relatively poor yaw control performance[1]. Reference 8 supports

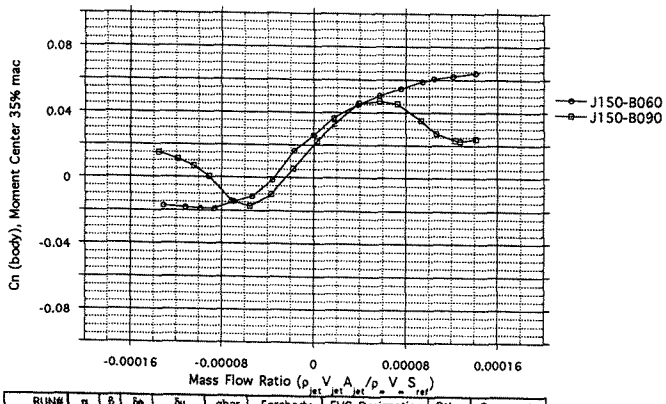


| RUN# | α | β | δφ | δμ | qbar | Forebody | FVC Designation | Other | Comments |
|---|---|---|---|---|---|---|---|---|---|
| 330-336 | 50° | 0 | --- | sweep | 20 | STANDARD | various | | jets |

**Figure 12. Effect of Nozzle Azimuth Standard Nose, FS 5**

this observation with a brief mention that blowing from outboard directed jets located at FS 45 did not produce any significant effects. Jets directed inboard were not tested in Ref. 8.

**Longitudinal Position**. Figure 12 shows two nozzle azimuth positions at the next forward location, FS 5. The most effective nozzle azimuth at this fuselage station appears to be 60° (i.e., pointing inboard and aft). Preliminary tests with the nozzles located at FS 25 showed a similar behavior with azimuth, but to produce the same yaw moment greater mass flow rates were required compared to the other locations.

There appears to be an optimum location for the jet and vortex interaction for maximum effect on the forebody vortex development. Too far forward and the natural forebody flow overpowers the disturbance from the jet; too far aft the vortices are too well established and large blowing rates are necessary to disturb the flowfield. In order to optimally place the jet efflux, the nozzle azimuth must vary with the nozzle longitudinal location. For example, as the jet position moves forward, the nozzle azimuth must be directed more aft for maximum effectiveness.

## Slots

Similar to jet blowing, forebody vortex control using slots has been explored by a number of investigators on different configurations[7]. Slot geometries can be grouped into two large categories based on the direction of the exit flow. Normal slots direct the jet perpendicular to the body and generally act as a spoiler. Tangential slots blow along the surface of the body or wing and use the Coanda effect or otherwise energize the boundary layer. The present work used only tangential slots to affect the forebody flow.

The slots were located on lines of constant surface slope and defined by the normal vector similar to the nozzles. For the standard and shark noses, the slots were on the 105° and 120° normal vector. The chine only fit on the 120° nose due to the contour modifications necessary to fair the slot installation, so this was the only slot radial position tested with the chine. The slots extended from FS 5 to FS 40 and were divided into 4 roughly equal length segments designated A, B, C, and D from front to rear. During testing, different segments were blocked off allowing variations in the slot length and longitudinal position. The slot locations are shown as heavy lines in Fig. 4.

**Slot Position and Length**. Yaw moment developed from blowing from the two forward slot segments individually is shown in Fig. 13. Slot A is the most forward segment and develops slightly larger yaw moments than slot B. It is not apparent on these figures but the slots exhibit the same reversed effect at low blowing rates that was seen with the inward jet blowing. During the preliminary tests, longer slot lengths formed by two or three

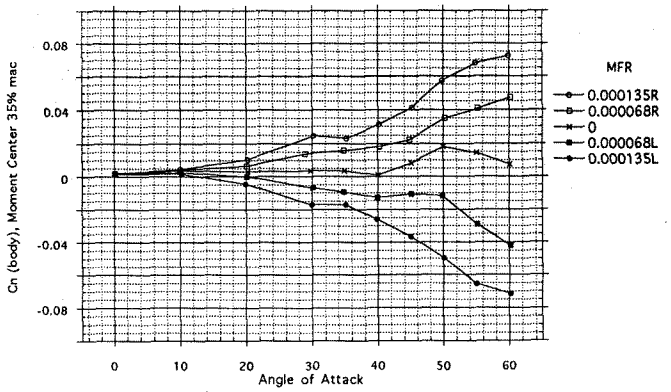


| RUN# | α | β | δφ | δμ | qbar | Forebody | FVC Designation | Other | Comments |
|---|---|---|---|---|---|---|---|---|---|
| 348-352 | sweep | 0 | --- | various | 20 | STANDARD | S105-A | | slots |

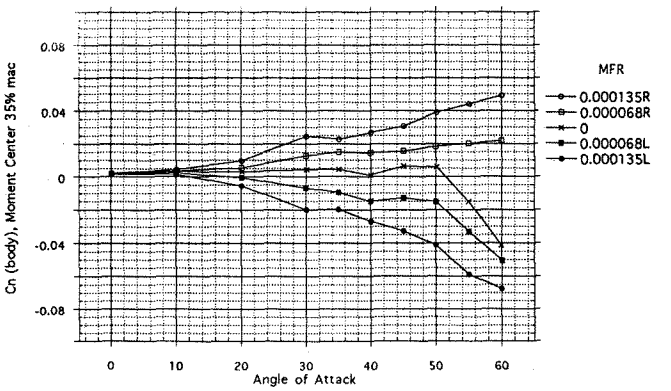


| RUN# | α | β | δφ | δμ | qbar | Forebody | FVC Designation | Other | Comments |
|---|---|---|---|---|---|---|---|---|---|
| 356-360 | sweep | 0 | --- | various | 20 | STANDARD | S105-B | | slots |

**Figure 13. Effect of Tangential Slots (a) First Segment, (b) Second Segment**

segments were tested. Compared to the single segment results, the reversed region was larger and more mass flow was required to produce the same yaw moment.

The yaw moment appears as if it might continue to increase with mass flow rates beyond the maximum tested. The maximum yaw control power could not be determined due to a limited blowing air supply. Possibly, the ultimate level might exceed that developed by jets but at a much larger flow rate. It should be mentioned that while a slot may or may not ultimately develop greater control power than a jet configuration, the practical application of either technique to an operational aircraft must take into account the mass flow requirements and efficiencies of producing control power.

**Slot Radial Position**. Two radial positions of the slot were tested in the preliminary wind tunnel entries. The radial position was not a large factor in slot performance with the standard nose, at least over the limited range covered in the two cases, 105° and 120°.

## CHINE NOSE

### Jets

Nozzle placement and azimuth on the chine nose had a larger significance than was seen with the standard nose. Figure 14 shows the effectiveness with angle of attack of the nozzles in the C position (FS 15) aimed forward and inboard at an azimuth angle of 150°. These configurations exhibited the now familiar characteristics of reversal at low blowing rates and high AOA and increasing effectiveness with angle of attack observed with the standard nose jets and slots.

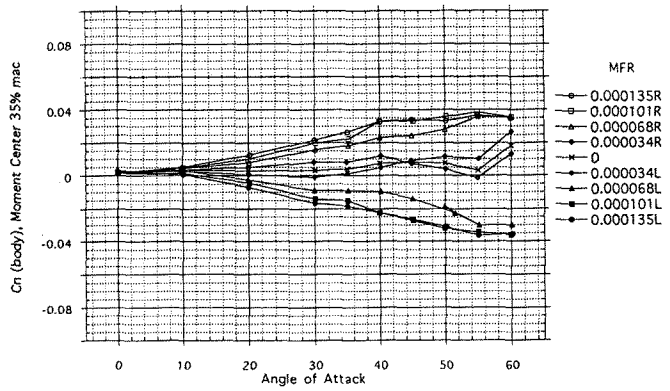


| RUN# | α | β | δφ | δμ | qbar | Forebody | FVC Designation | Other | Comments |
|---|---|---|---|---|---|---|---|---|---|
| 279-287 | sweep | 0 | --- | various | 20 | CHINE | J150-C150 | | jets |

**Figure 14. Jet Blowing on Chine Nose**

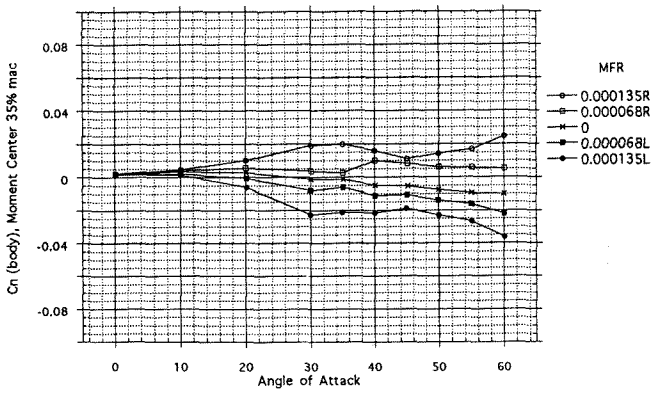


| RUN# | α | β | δφ | δμ | qbar | Forebody | FVC Designation | Other | Comments |
|---|---|---|---|---|---|---|---|---|---|
| 365-369 | sweep | 0 | --- | various | 20 | CHINE | S120-C | | slots |

**Figure 15. Slot Blowing on Chine Nose**

### Slots

The only slot segment that produced a significant yaw moment with the chine nose was segment C (see Fig. 15). This is counter to the findings with the standard nose where the most forward segment was most effective. Segment C's position near the aft end of the chine allowed it to influence the forebody flow, whereas the more forward segments' effects were engulfed by the massive disturbance of the chine. Figure 15 shows no reversal at low blowing rates. This may be due to the "separator" effect of low blowing rates suggested earlier also being overwhelmed by the presence of the chine. Larger mass flow rates than possible in this experimental set-up may ultimately produce greater yaw moments but again the relative "inefficiency" of the slot compared to the jet must be noted.

## SHARK NOSE

### Jets

Preliminary investigations with jet blowing on the shark nose at three different longitudinal positions showed similar trends of dependency between longitudinal position and optimum nozzle angle that was apparent with the standard nose. The most forward position, location A, developed the maximum control power when the nozzle was pointed inboard and aft. At the next position, B, a nozzle azimuth of 90° had the best performance. Moving to the C longitudinal location, the jets produced the largest yaw moments when pointing forward and inboard.

Figure 16 shows the jets in the C position (FS 15) at an azimuth of 120°. At equal blowing rates the yaw moment developed is more than 50% greater than with the chine nose and almost as large as produced with the standard nose. Low blowing rates at high AOA produced the reversal in effectiveness that was seen with the standard nose.

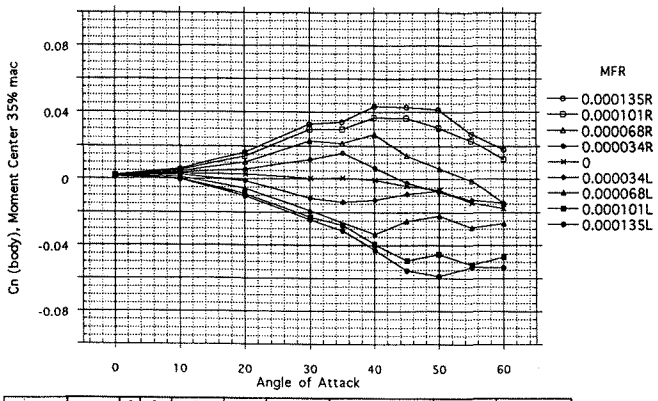


| RUN# | α | β | δφ | δμ | qbar | Forebody | FVC Designation | Other | Comments |
|---|---|---|---|---|---|---|---|---|---|
| 665-673 | sweep | 0 | --- | various | 20 | SHARK | J150-C120 | LEX3, LSB | jets |

**Figure 16. Jet Blowing on Shark Nose**

## MECHANICAL FVC

Early flow visualization studies revealed small vortices being shed into the wake behind a nose boom from each diameter increase. In some instances the shed vortices have been observed to promote symmetric development of the forebody vortices; in other cases the vortices interact with an adverse result. A well-studied technique of controlling the nose boom wake and therefore the forebody vortices is by installing small strakes on the nose boom[9]. These observations, along with the well-known sensitivity of the leeward vortices of a slender forebody to small external disturbances, lead to the idea of a small, variable disturbance mounted on the nose boom for the purpose of actively controlling the formation of the forebody vortices. Water tunnel flow visualization studies qualitatively confirmed the ability of a single miniature strake to affect the forebody vortices' position[10]. The wind tunnel tests discussed here focused on a parametric study of the strake design variables and a quantitative assessment of the strake performance.

During the preliminary wind tunnel investigation a large variety of strake geometries was tested. The baseline strake, designated as Strake "A," had a leading-edge sweep of 80°, trailing-edge sweep of 40° (swept forward) and an exposed chord of 4.5" full-scale. Geometry variations examined in the preliminary tests included: leading-edge sweeps of 75° and 70°, and trailing-edge sweeps of 0°, 20°, 40°, and 60°. Dual strake configurations had included angles of 90°, 120°, 150°, and 180° (at zero strake rotation, equivalent to dihedral angles of $\Gamma$ = -45°, -30°, -15°, and 0° respectively).

A motor driven mechanism allowed the strake rotation angle to be changed remotely while the tunnel was in operation. The strakes were mounted on a removable sleeve that rotated around the nose boom. The boom was fixed to the fuselage and did not rotate with the strakes, thereby eliminating any varying effect of imperfections of the boom. Different strake geometries were fabricated on interchangeable sleeves simplifying configuration changes. The strake rotation angle was sensed by a multi-turn precision potentiometer located in the forward nose section. Positive rotation is counter-clockwise from the pilot's perspective. Zero rotation angle was defined as a symmetric placement; a single strake on the windward meridian or dual strakes equally displaced to each side.

## STANDARD NOSE

### Single Strake

The strake becomes effective at angles of attack above 30° as shown in Fig. 17. At angles of attack below 30° there is not an appreciable vortex formation on the forebody for the strake to effect. As the angle of attack increases, so does the forebody vortex strength and consequently maximum control effectiveness. The apparent decrease in control power above 55° AOA may be due to the forward movement of the vortex burst with angle of attack. The useful control range of all the strakes is between ±45°, and the maximum yaw moment peak-to-peak magnitude is about 0.08.

**Planform Changes**. Parametric variations to the strake geometry were tested in the preliminary wind tunnel series[2]. Planform changes had a small effect on the performance of the single strake. The upper graph in Fig. 18 shows the effects of a variation in leading-edge sweep of 80°, 75° and 70° with a constant trailing-edge sweep. Strake spans and areas also changed with leading-edge sweep. The variation in leading-edge sweep shows only a small change in the control gradient and has little effect on the maximum magnitude over the useful range. Likewise, as shown in the lower graph, trailing-edge sweep variations result in little change in the control characteristics of

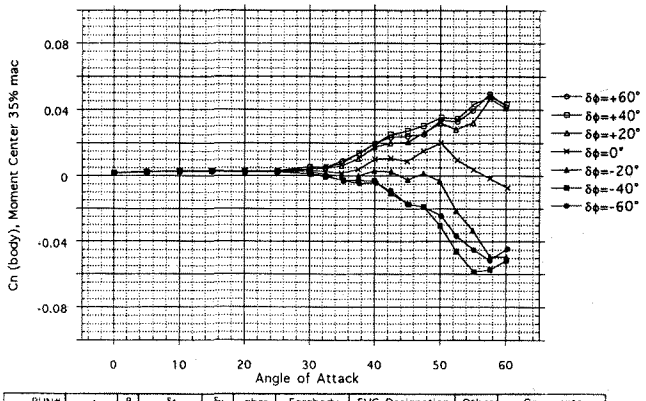


| RUN# | α | β | δφ | δμ | qbar | Forebody | FVC Designation | Other | Comments |
|---|---|---|---|---|---|---|---|---|---|
| 128-134 | sweep | 0 | -60 +60 | --- | 20 | STANDARD | A-aft | | single strake aft |

**Figure 17. Mechanical FVC with Standard Nose**

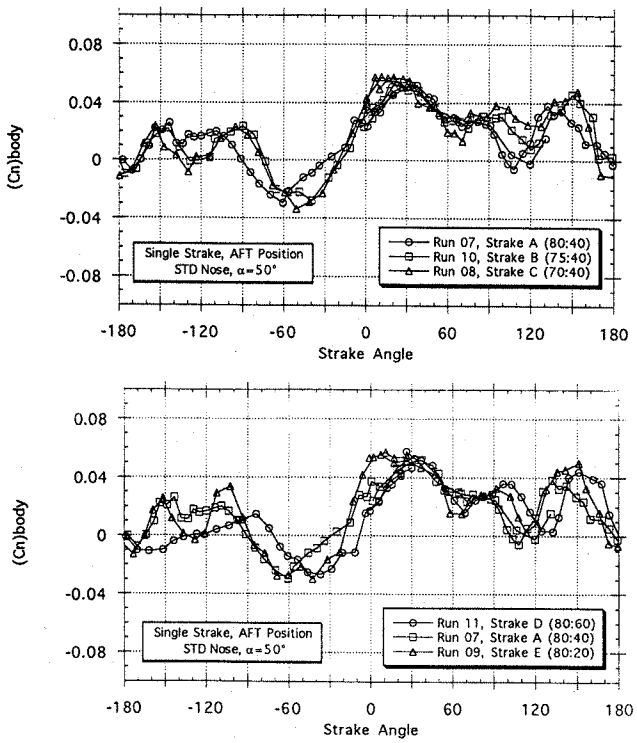


**Figure 18. Strake Sweep Effect (a) Leading Edge, (b) Trailing Edge**

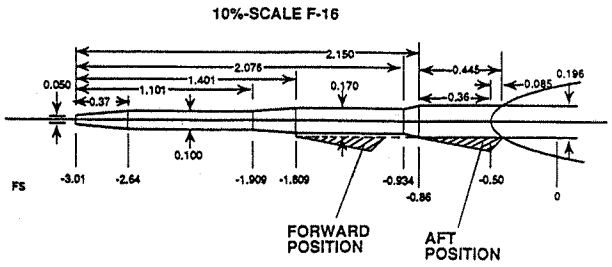


**Figure 19. Strake Longitudinal Positions**

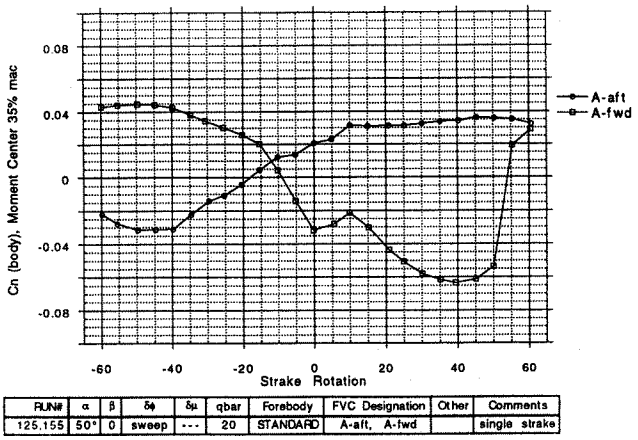


| RUN# | α | β | δφ | δμ | qbar | Forebody | FVC Designation | Other | Comments |
|---|---|---|---|---|---|---|---|---|---|
| 125.155 | 50° | 0 | sweep | --- | 20 | STANDARD | A-aft, A-fwd | | single strake |

**Figure 20. Effect of Strake Longitudinal Position**

the single strake. The different levels of yawing moment at zero strake rotation are due to imperfections and asymmetries in the strake fabrication.

**Longitudinal Position**. By lengthening the rotation sleeve to which the strake is attached, the strake longitudinal location on the boom can be varied. The sketch in Fig. 19 shows the single strake in the forward and aft positions. Figure 20 shows the single strake in the aft position presented previously, along with the strake in the forward position. Moving the strake between the aft and forward positions completely reverses the direction of the generated yaw moment. In the aft position, a positive deflection (counter-clockwise as seen by the pilot) produces a positive yaw moment. In the forward position the same positive deflection produces a negative yaw moment. The magnitude of the total moment variation is slightly larger with the strake in the forward position.

Fluorescent oil flow visualization showed that the aft positioned strake shed a vortex that was captured by the forebody vortex on the same side, thereby strengthening that vortex. When the strake was moved forward on the boom, the strake vortex flowed off the strake, up onto the leeward side of the boom, then crossed over the forebody to energize the opposite side forebody vortex. The opposite side vortex strengthening causes the observed reversed control gradient.

The ability to select the sign of the control gradient by the longitudinal placement of the strake offers the aerodynamicist some degree of flexibility. Assuming that a negative strake roll angle is equivalent to a positive sideslip, then a negative control gradient (from a single strake in the forward position) would generate more positive $Cn_\beta$ increasing the static directional stability. Conversely, a positive control gradient (single strake aft) would be expected to augment yaw damping.

**Yawed Conditions** . The control effectiveness and character are retained in sideslip as shown by Fig. 21 with the single strake in the aft position at 50° AOA and 0° and ±10° sideslip.

## Dual Strake

Slender ogive bodies of revolution exhibit almost step-like changes in side force as the body is rolled. Water tunnel investigations with the single rotatable strake also showed a high sensitivity to the strake rotation around zero degrees causing sudden switching of the vortex asymmetries. This is not a very useful characteristic for a flight control device. The dual strake configuration was conceived to provide a moderation of the control gradient through the interference of the two strakes. It was desired to find an arrangement of strakes that first interferes with

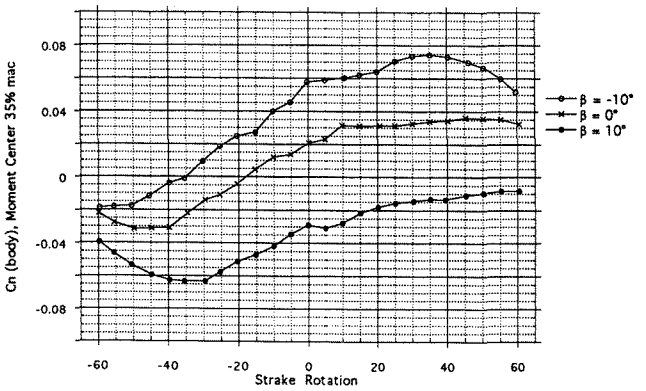


| RUN# | α | β | δφ | δμ | qbar | Forebody | FVC Designation | Other | Comments |
|---|---|---|---|---|---|---|---|---|---|
| 125, 149-150 | 50° | -10°, 10° | sweep | --- | 20 | STANDARD | A-aft | | single strake aft |

**Figure 21. Single Strake in Yaw**

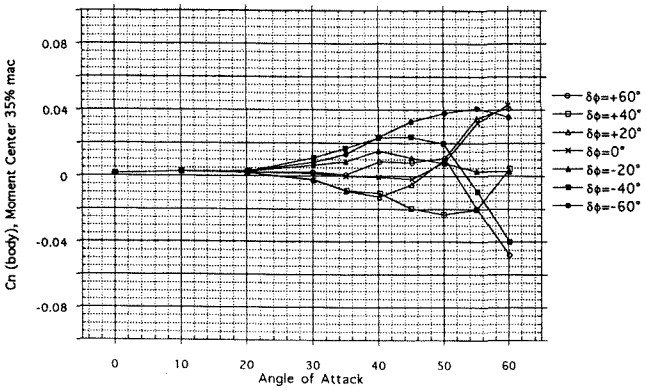


| RUN# | α | β | δφ | δμ | qbar | Forebody | FVC Designation | Other | Comments |
|---|---|---|---|---|---|---|---|---|---|
| 194-200 | sweep | 0 | -60° to 60° | --- | 20 | STANDARD | A150-aft | | dual strake aft |

**Figure 22. Dual Strake with Standard Nose**

each other to produce a well-behaved control gradient and then compliments each other and produces greater maximum yaw moments.

**Dihedral Effects**. The included angle of the dual strake configuration has a strong effect on the performance as shown in the preliminary tests[2]. Figure 22 shows the performance of the dual strakes with an included angle of 150°. The maximum yaw moment is larger than that developed with a single strake, but the behavior is somewhat confused at high angles of attack and may not be useful as a control device. Apparently, the interactions between the two strake vortices and the forebody vortices are complex.

## CHINE NOSE

Preliminary tests showed the ineffectiveness of miniature nose boom strakes on the chined configuration. Surface pressure measurements revealed that the flow on the forebody lee side is largely separated due to the chine and that effects of the forebody vortices were very weak. The strakes were unable to overcome the dominating influence of the chine on the forebody flowfield.

## SHARK NOSE

### Single Strake

In contrast to the chine nose, the single strake is still an effective yaw moment generator with the shark nose. The upper portion of Fig. 23 shows the yaw moment response with varying strake angle. The control gradient increases with angle of attack. The control power is about 2/3 that developed with the standard nose. Significant yaw control is not available until the angle of attack is greater than 45° as shown in the lower figure.

### Dual Strake

Figure 24 shows a dual strake arrangement. The behavior is more as expected with a consistent response over the angle of attack range. The control gradients for this particular configuration are greater than with the single strake. This has potential advantages and disadvan-

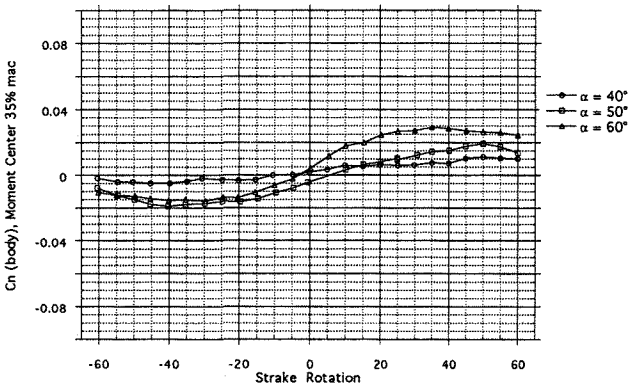


| RUN# | α | β | δφ | δμ | qbar | Forebody | FVC Designation | Other | Comments |
|---|---|---|---|---|---|---|---|---|---|
| 374-377 | 40°, 50°, 60° | 0 | sweep | --- | 20 | SHARK | A-aft | | single strake aft |

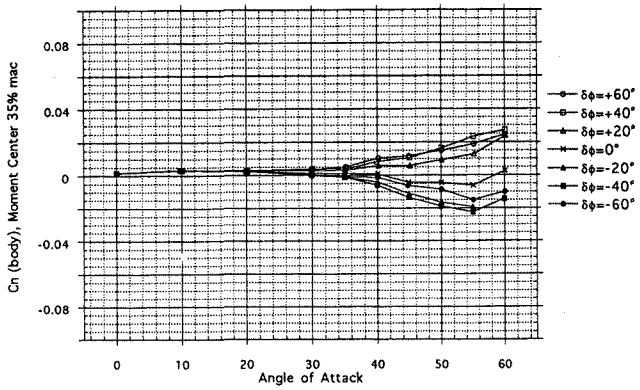


| RUN# | α | β | δφ | δμ | qbar | Forebody | FVC Designation | Other | Comments |
|---|---|---|---|---|---|---|---|---|---|
| 378-384 | sweep | 0 | -60° to 60° | --- | 20 | SHARK | A-aft | | single strake aft |

**Figure 23. Single Strake with Shark Nose**

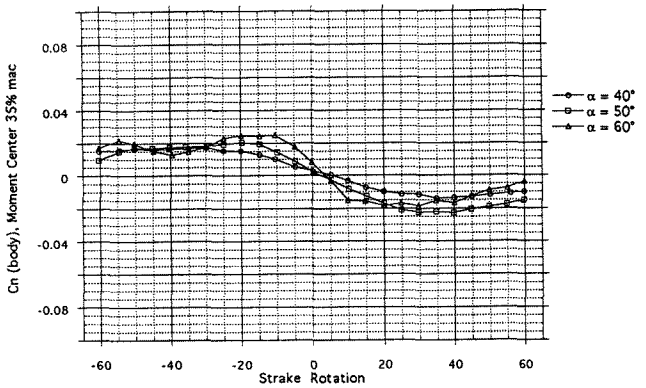


| RUN# | α | β | δφ | δμ | qbar | Forebody | FVC Designation | Other | Comments |
|---|---|---|---|---|---|---|---|---|---|
| 402-404 | 40°, 50°, 60° | 0 | sweep | --- | 20 | SHARK | A120-aft | | dual strake aft |

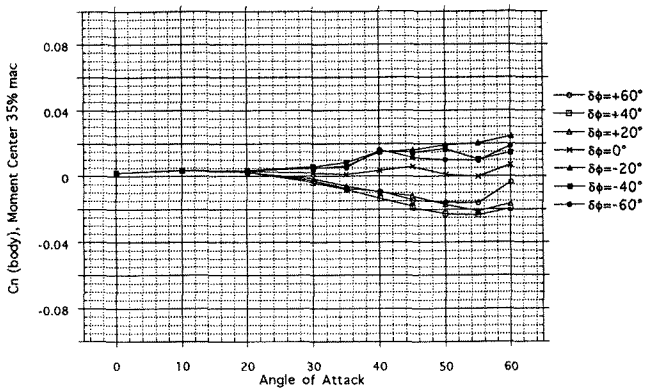


| RUN# | α | β | δφ | δμ | qbar | Forebody | FVC Designation | Other | Comments |
|---|---|---|---|---|---|---|---|---|---|
| 405-411 | sweep | 0 | -60° to 60° | --- | 20 | SHARK | A120-aft | | dual strake aft |

**Figure 24. Dual Strake with Shark Nose**

tages. A steep gradient means less deflection of the strakes is required to produce a desired yaw moment, but it might be more sensitive to sideslip or disturbances.

The differences in dual strake behavior with the standard and shark noses suggest that some degree of stabilization or separation of the forebody vortices was provided by the shark nose that was not available with the more circular cross-section of the standard F-16. A circular cross-section is likely to have a bi-stable vortex formation that would be more sensitive to interference effects. The dual strake FVC technique is viable with the shark nose, perhaps because of an increased independence of the forebody vortices.

## HIGHLIGHTS OF RESULTS

On the basis of these wind tunnel tests of the F-16 the following conclusions have been drawn:

### Nose Modifications:

- The standard nose F-16 exhibits a static yaw instability at angles of attack above 30°. The addition of the chine results in a stable configuration. The shark nose is neutral or stable directionally over the angle of attack range.
- Both the chine and shark noses experience less asymmetric yaw moment at zero sideslip conditions than the standard F-16 nose.

### Pneumatic FVC:

- Both pneumatic forebody vortex control techniques were effective with all three nose shapes.
- Jets angled across the body worked best. There is an optimum region for influencing the flowfield. Nozzles in forward positions need to point inward and aft, while nozzles in aft locations must point inward and forward for maximum effect.
- The jets demonstrated yaw control power at high angles of attack similar to the levels obtainable with conventional controls at low angles of attack.
- The shortest and most forward slot position was most effective. The slot performance was relatively unchanged between the two radial positions tested.
- To develop the same yaw moment, the slots required more mass flow than the jet configurations.
- Jets and slots were effective over a large angle of attack range and the effectiveness increased with angle of attack. Conventional yaw control power decreases substantially at high angles of attack.

### Mechanical FVC:

- Rotating nose boom strakes are an effective source of yaw moment at angles of attack above 40°, producing approximately the equivalent to the maximum control power available from the rudder at any angle of attack.

- The magnitude and character of the yaw moment are relatively unaffected by strake planform variations. The longitudinal position of the strakes along the boom had a major effect on both the magnitude and gradient of the control. The included angle of the dual strake arrangement also had a large effect on the character of the yaw moment response.

- The rotating nose boom strakes were ineffective with the chine configuration.

- Nose boom strakes are an effective yaw control with the shark nose and at high angles of attack develop roughly 50% of the maximum control moments of conventional controls.

Overall, both pneumatic and mechanical methods of forebody vortex control are viable sources of yaw moment for control. Pneumatic forebody vortex control systems are effective with all three nose configurations with jets being more efficient at a given mass flow than the slot configurations. The rotating nose boom strake control system is effective with the standard and shark nose configurations.

## ACKNOWLEDGMENTS

This research was sponsored by NASA Langley Research Center under the SBIR program, Contract NAS1-19584 and by the Flight Dynamics Directorate of Wright Laboratory. The NASA technical monitor was Mr. Dan Banks. Capt. Neal Mosbarger (WL/FIMM) provided on-site support during the wind tunnel tests. We also wish to acknowledge the craftsmanship of Eidetics' model builder, Bert Ayers and the innumerable contributions from Gerald Malcolm, Brian Kramer, Carlos Suárez and Dr. Terry Ng.

## REFERENCES

1. Smith, B. C., and Ng, T. T., "Pneumatic Control of Vortices on Different F-16 Forebodies Using Jets and Slots," AIAA 94-0049, 1994.

2. Smith, B. C., and Ng, T. T., "Mechanical Control of Vortices on Different F-16 Forebodies Using Miniature Rotating Strakes," AIAA 94-0048, 1994.

3. Lee, C. J., Tavella, D., Wood, N. J., and Roberts, L., "Flow Structure and Scaling Laws in Lateral Wing-Tip Blowing," AIAA Journal, Vol. 27, No. 8, 1989, pp. 1002-1007.

4. Meyn, L. A., Lanser, W. R., and James, K. D., "Full-Scale High Angle-of-Attack Tests of an F/A-18," AIAA 92-2676, 1992.

5. Kramer, B. R., Suárez, C. S., Malcolm, G. N., and James, K. D., "Forebody Vortex Control with Jet and Slot Blowing on an F/A-18," AIAA 93-3449, 1993.

6. Guyton, R. W., and Maerki, G., "X-29 Forebody Jet Blowing," AIAA 92-0017, 1992.

7. Malcolm, G. N., "Forebody Vortex Control - A Progress Review," AIAA 93-3540, 1993.

8. LeMay, S. P., Sewall, W. G., and Henderson, J. F., "Forebody Vortex Flow Control using Tangential Slot and Jet Blowing," AIAA 92-0019, 1992.

9. Brandon, J. M., "Low-Speed Wind-Tunnel Investigation of the Effect of Strakes and Nose Chines on Lateral-Directional Stability of a Fighter Configuration," NASA TM-87641, 1986.

10. Suárez, C. J., Malcolm, G. N., and Ng, T. T., "Forebody Vortex Control with Miniature, Rotatable Nose-Boom Strakes," AIAA 92-0022, 1992.